1521-009X/46/9/1320–1328$35.00
Drug Metabolism and Disposition

https://doi.org/10.1124/dmd.118.081182
Drug Metab Dispos 46:1320–1328, September 2018

Differences in the In Vivo and In Vitro Metabolism of Imrecoxib in Humans: Formation of the Rate-Limiting Aldehyde Intermediate

Xiangyu Hou, Jialan Zhou, Songda Yu, Lei Zhou, Yifan Zhang, Dafang Zhong, and Xiaoyan Chen

Shanghai Institute of Materia Medica, Chinese Academy of Sciences, Shanghai, China (X.H., J.Z., S.Y., L.Z., Y.Z., D.Z., X.C.); and University of Chinese Academy of Sciences, Beijing, China (X.H., D.Z., X.C.)

Received February 28, 2018; accepted June 29, 2018

ABSTRACT

Imrecoxib is a typical cyclooxygenase-2 inhibitor and the benzylic carbon motif is its major site of oxidative metabolism, producing a hydroxymethyl metabolite (M1) and a carboxylic acid metabolite (M2). The plasma exposure of M2 is four times higher than those of both M0 and M1 in humans. However, this metabolite is rarely formed in in vitro experiments. Therefore, this study aims to investigate the formation mechanism of M2 and to further elucidate the reason for the discrepancy between in vitro and in vivo metabolic data. By employing human hepatocytes, human liver microsomes (HLMs), human liver cytosols (HLCs), recombinant enzymes, and selective enzyme inhibitors, the metabolic map of imrecoxib was elaborated as follows: the parent drug was initially hydroxylated to form M1 in HLMs, mainly mediated by CYP3A4 and CYP2D6, and to subsequently form aldehyde imrecoxib (M-CHO) in HLMs and HLCs. The latter process is the rate-limiting step in generating the end-product M2. In further M-CHO metabolism, two opposite reactions (namely, rapid oxidation catalyzed by CYP3A4, CYP2D6, and cytosolic aldehyde oxidase to form M2 versus reduction to regenerate M1 mediated by NADPH-dependent reductases in HLMs and HLCs, such as cytochrome P450 reductase) led to marked underestimation of the M2 amount in static in vitro incubations. The findings provided a possible explanation for the difference between in vitro and in vivo metabolism of imrecoxib, suggesting that the effect of competitive reduction on the static oxidation metabolism in in vitro metabolic experiments should be considered.

Introduction

Coxibs are widely used in clinical practice as nonsteroidal anti-inflammatory drugs for alleviating pain based on their inhibition of cyclooxygenase-2. Typical marketed coxibs such as celecoxib and etoricoxib both contain the aromatic methyl group, which is their major site of oxidative metabolism, producing a hydroxymethyl metabolite with subsequent oxidation to the corresponding carboxylic acid metabolite (Paulson et al., 2000; Rodrigues et al., 2003). CYP2C9 is reportedly involved in the formation of hydroxymethyl celecoxib (Tang et al., 2000, 2001), and alcohol dehydrogenase is responsible for further metabolism to carboxy-celecoxib (Sandberg et al., 2002).

Similar to celecoxib, imrecoxib (another moderately selective cyclooxygenase-2 inhibitor approved in 2011) also contains a *para*-benzyl fraction. The metabolism of imrecoxib in rats has been investigated (Xu et al., 2006a,b). Imrecoxib undergoes a two-step oxidation of benzylic carbon and successively forms a hydroxymethyl metabolite (M1) and a carboxylic acid metabolite (M2), which are both confirmed to exhibit similar pharmacological activity to the parent drug (Feng et al., 2009). However, the metabolism of imrecoxib in humans has not been reported.

The design of drug-drug interaction clinical trials is essential for the clinical use of imrecoxib. Thus, understanding the principal metabolizing routes and identifying the enzymes involved are of considerable importance. Our pilot experiment indicated that the major metabolites of imrecoxib in humans after an oral administration are M1 and M2 by a two-step successive oxidization. M2 is the prominent drug-related component in both plasma and urine. However, this metabolite is seldom formed in human liver microsomes (HLMs) in in vitro experiments. Therefore, another objective of the study was to explore the formation mechanism of M2 so as to further elaborate the cause for the discrepancy between in vitro and in vivo metabolic data.

Materials and Methods

Chemicals and Reagents. Reference substances of imrecoxib, M1, M2, and the internal standard (IS) 3-(4-methoxyphenyl)-4-(4-(methylsulfonyl)phenyl)-1-propyl-1*H*-pyrrol-2(5*H*)-one (BAP385) were kindly provided by Jiangsu Hengrui Medicine Co. Ltd. (Lianyungang, China). Pooled HLMs, human liver cytosols (HLCs), and recombinant cytochrome P450 (P450) enzymes [CYP1A2, CYP2A6, CYP2B6, CYP2C8, CYP2C9, CYP2C19, CYP2D6, CYP2E1, CYP3A4, and CYP3A5, all containing P450 reductase (POR) and cytochrome-b_5] were supplied by BD Gentest (Woburn, MA). Human NADPH-POR, human CYP3A4R (without cytochrome-b_5), and human CYP3A4BLR (with cytochrome-b_5 and low-activity POR) were purchased from Cypex Ltd. (Dundee, Scotland, UK).

This work was supported by the National Natural Science Foundation of China [Grant 81573500] and the Strategic Priority Research Program of the Chinese Academy of Sciences [Grant XDA 12050306].
https://doi.org/10.1124/dmd.118.081182.
This article has supplemental material available at dmd.aspetjournals.org.

ABBREVIATIONS: ABT, 1-aminobenzotriazole; ALDH, aldehyde dehydrogenase; AOX, aldehyde oxidase; BAP385, 3-(4-methoxyphenyl)-4-(4-(methylsulfonyl)phenyl)-1-propyl-1*H*-pyrrol-2(5*H*)-one; ETC, electron transport chain; HLC, human liver cytosol; HLM, human liver microsome; IS, internal standard; JWH-018, 1-pentyl-3-(1-naphthoyl)indole; M-CHO, aldehyde imrecoxib; *m/z*, mass-to-charge ratio; MS, mass spectrometry; NMR, nuclear magnetic resonance; P450, cytochrome P450; PBS, phosphate-buffered saline; POR, cytochrome P450 reductase; SGX523, 6-[[6-(1-methylpyrazol-4-yl)-[1,2,4]triazolo[4,3-*b*]pyridazin-3-yl]sulfanyl]quinoline; UPLC, ultra-performance liquid chromatography; XO, xanthine oxidase.

Cryopreserved primary human hepatocytes were obtained from XenoTech (Lenexa, KS). NADPH, NAD, NADP, α-lipoic acid, and 1-aminobenzotriazole (ABT) were purchased from Sigma-Aldrich (St. Louis, MO). References of menadione and methoxyamine were obtained from Meilunbio (Dalian, China). All other reagents and solvents were either analytical or high-performance liquid chromatography grade.

Aldehyde imrecoxib (M-CHO) was synthesized as follows: 1,1-dihydro-1,1,1-triacetoxy-1,2-benzoiodooxol-3(1H)-one (Dess-Martin reagent, 11 mg, 0.026 mmol) was added to a solution of M1 (5 mg, 0.013 mmol) in dichloromethane at 0°C, and the mixture was stirred for 30 minutes. Then the reaction was quenched with $NaHCO_3$-saturated aqueous solution. The organic layer was separated and washed with NaCl saturated aqueous solution, dried over Mg_2SO_4, then filtered and concentrated. The obtained residues were purified with preparative thin-layer chromatography [dichloromethane/methanol = 20:1 (v/v)] to yield a white solid. The structure was confirmed based on nuclear magnetic resonance (NMR) and mass spectrometry (MS) data. ^{1}H NMR (400 MHz, chloroform-*d*) δ 10.03 (s, 1H), 7.92–7.85 (m, 4H), 7.58 (d, J = 8.2 Hz, 2H), 7.45 (d, J = 8.5 Hz, 2H), 4.37 (s, 2H), 3.58 (t, J = 7.4 Hz, 2H), 3.08 (s, 3H), 1.73 (h, J = 7.4 Hz, 2H), and 1.01 (t, J = 7.4 Hz, 3H). ^{13}C NMR (126 MHz, Chloroform-d) δ 191.98, 169.39, 146.82, 141.37, 138.49, 137.56, 136.34, 134.74, 130.4 (2C), 130.10 (2C), 128.75 (2C), 128.25 (2C), 52.84, 44.58, 44.56, 22.11, 11.64. High-resolution MS (electrospray ionization): mass-to-charge ratio (*m/z*) $[M-H]^-$ calculated for $C_{21}H_{20}NO_4S^-$, 382.1119; found, 382.1120.

Individual stock solutions of imrecoxib, M1, M-CHO, and other inhibitors were prepared by dissolving each compound in dimethylsulfoxide. The stock solutions were then diluted with 100 mM phosphate-buffered saline (PBS; pH 7.4) containing $MgCl_2$ (0.5 mM) or Williams' E medium to the desired concentrations [with a final organic content of 0.1% (v/v), except for α-lipoic acid, which required 10% (v/v), due to the poor water solubility; the same organic content was retained for the controls].

Instruments. Metabolite profiling was performed on an Acquity ultra-performance liquid chromatography (UPLC) system (Waters Corp., Milford, MA) coupled with a TripleTOF 5600$^+$ system (AB Sciex, Concord, ON, Canada). NMR spectra of M-CHO confirmation were recorded on a Bruker Avance III 400 spectrometer (Newark, DE). Quantitation analysis of imrecoxib and its metabolites was conducted using an API 5500 triple quadrupole mass spectrometer coupled with an LC-30AD high-performance liquid chromatography system (Shimadzu, Kyoto, Japan). Data acquisition and processing was conducted using Analyst 1.6.2 software (AB Sciex).

Animals. Male Sprague-Dawley rats (200 ± 20 g) were purchased from Sipper-BK laboratory Animal Co. Ltd. (Shanghai, China). All animal studies were performed in accordance with the principles of the Animal Care and Use of Laboratory Committee of the Shanghai Institute of Materia Medica, Chinese Academy of Sciences (Shanghai, China). The rats were divided into three groups randomly (n = 5/group). Imrecoxib, M1, and M-CHO were intravenously administered separately to each group at a dose of 5 mg/kg. Then blood was drawn from the retro-orbital venous before dosing (0 hours) and at 5, 15, and 30 minutes and at 1, 1.5, 2, 4, 7, and 10 hours postdosing. Plasma was obtained by centrifugation at 11,000*g* for 10 minutes and stored at −80°C until analysis.

Human Study and Sample Collection. This study was conducted in accordance with the Declaration of Helsinki and the principles of Good Clinical Practice and was approved by the Ethics Committee of the Xijing Hospital, affiliated with the Fourth Military Medical University (Xi'an, China). All participants signed informed consent forms prior to the study. The participants received a single dose of 100 mg imrecoxib orally in fed states. Blood samples were collected before dosing (0 hours) and at 0.5, 1, 2, 3, 4, 6, 8, 12, 24, 36, 48, 72, and 96 hours postdosing. Plasma was harvested after centrifugation of blood at 11,000*g* for 10 minutes. Urine samples were collected predosing (−2 to 0 hours) and at 0–2, 2–4, 4–8, 8–12, 12–24, 24–48, 48–72, and 72–96 hours postdose, and the volume of individually collected samples was measured and recorded. Both the plasma and urine samples were stored at −80°C until analysis.

Sample Preparation and UPLC-UV/Quadrupole Time-of-Flight MS Analysis. An aliquot of 100 μl of sample was mixed with 400 μl acetonitrile, followed by vortexing for 1 minute and centrifugation at 14,000 rpm for 5 minutes. The supernatant was evaporated to dryness under an N_2 stream at 40°C. The residues were reconstituted with 100 μl acetonitrile/water [10:90 (v/v)]. Then 7 μl of the mixture was injected into the UPLC quadrupole time-of-flight MS system for analysis. Chromatographic separation was performed on an Acquity UPLC HSS T3 column (100 × 2.1 mm i.d., 1.8 μm; Waters). The mobile phase was a mixture of 5 mM ammonium acetate containing 0.1% (v/v) formic acid (A) and acetonitrile (B). Gradient elution started from 5% B, linearly increased to 15% B within 2.5 minutes, to 20% B within the subsequent 2.5 minutes, to 32% B in 5 minutes, and to 90% B in 2 minutes and was then maintained for 1 minute and finally adjusted to 5% B for 3 minutes to re-equilibrate the column. The flow rate was set at 0.4 ml/min, and the column temperature was maintained at 40°C. The eluent was monitored by UV detection at 300 nm.

MS detection was conducted with electrospray ionization via a DuoSpray ion source (AB Sciex) in positive mode. The parameter settings were as follows: temperature, 500°C; curtain gas, 40 (arbitrary units); ion source gas 1 and gas 2, 55 (arbitrary units); ion-spray voltage floating, 5.5 kV; declustering potential, 80 V; collision energy, 10 eV; and collision energy for product ion, 46 eV. The instrument was calibrated before the sample run and automatically calibrated after every five injections. Accurate mass spectra were acquired in the *m/z* range of 100–1000. Data were acquired via an information-dependent acquisition method, which was performed using Analyst TF 1.6. MetabolitePilot software (AB Sciex), a tool for profiling and characterizing metabolites.

Determination of Imrecoxib, M1, M2, and M-CHO. After acetonitrile-induced protein precipitation of samples, 10 μl of the mixture was injected into the liquid chromatography–MS/MS system for analysis. The analytes and IS were separated on an Eclipse Plus-C18 column (100 × 4.6 mm i.d., 3.5 μm; Agilent, Santa Clara, CA). Column temperature was maintained at 40°C. The mobile phase consisted of 5 mM ammonium acetate, formic acid, and acetonitrile [35:0.1:65 (v/v/v)] at the flow rate of 0.7 ml/min. Detection was operated in the positive multiple reaction monitoring scan mode by using a dwell time of 100 milliseconds per transition to detect ion pairs at *m/z* 370→236 (imrecoxib), 386→236 (M1), 400→236 (M2), 384→236 (M-CHO), and 386→278 (IS). The spray voltage and source temperature were set to 5500 V and 500°C, respectively.

In Vitro Incubations of Imrecoxib and M1. NADPH (2.0 mM) was preincubated with HLMs (0.5 mg/ml) or PBS for the control at 37°C for 10 minutes; then 10 μM imrecoxib and M1 were separately added to initiate their individual reactions. After 90 minutes of incubation, the reactions were terminated by adding an equal volume of ice-cold acetonitrile. To further confirm the participation of P450 enzymes, 10 isoforms of recombinant human P450 enzymes (50 pM; namely, CYP1A2, CYP2A6, CYP2B6, CYP2C8, CYP2C9, CYP2C19, CYP2D6, CYP2E1, CYP3A4, and CYP3A5) were separately incubated with imrecoxib (3.0 μM) in the presence of NADPH for 90 minutes. The operation procedures and conditions were similar to those for incubation with HLMs, except HLMs were replaced by each recombinant human P450 enzyme. The normalized relative contribution of each P450 was calculated according to the method reported previously (Rodrigues, 1999). Incubations of specific-chemical inhibitors (2 μM α-naphthoflavone, 6 μM quercetin, 1 mM ABT, 6 μM sulfaphenazole, 8 μM quinidine, 24 μM ticlopidine, 24 μM clomethiazole, and 2 μM ketoconazole) of each P450 enzyme in HLMs with imrecoxib were conducted separately using the similar protocol mentioned above.

To determine the effects of HLC enzymes, HLC (0.5 mg/ml) was preincubated with or without NAD at 37°C for 10 minutes. Afterward, 10 μM imrecoxib or M1 was added to start the reaction. After 90 minutes of incubation, the reactions were quenched by the addition of ice-cold acetonitrile.

The metabolism of imrecoxib and M1 was also evaluated in human hepatocytes. Each compound (10 μM) was incubated with human hepatocytes (1.0×10^6 cells/ml) in Williams' E medium for 3 hours at 37°C, in the absence or presence of ABT. The reactions were quenched by an equal volume of ice-cold acetonitrile. Each experiment was performed in duplicate.

In in vitro incubations, probe substrates [phenacetin, bupropion, paclitaxel, tolbutamide, *S*-mephenytoin, dextromethorphan, midazolam, testosterone, and SGX523 (6-[[6-(1-methylpyrazol-4-yl)-[1,2,4]triazolo[4,3-*b*]pyridazin-3-yl]-sulfanyl]quinoline)] were selected as positive controls to prove the activity of each enzyme as well as the potency and selectivity of the chemical inhibitors.

Trapping of M-CHO in HLMs, HLCs, and Recombinant P450s. Trapping reagent methoxyamine (10 mM) was incubated with NADPH-fortified (2 mM) HLMs (0.5 mg/ml) or HLCs (0.5 mg/ml). After 10 minutes of preincubation at 37°C, 10 μM M1 was added to initiate the 90-minute reactions, which were terminated using an equal volume of ice-cold acetonitrile. Trapping experiments were also performed to identify the enzyme phenotyping for M-CHO formation, in which HLMs or HLCs were replaced by NADPH-fortified recombinant P450s. The chromatographic peak areas of M-CHO–methoxyamine adduct detected in P450 incubations were compared with each other.

In Vitro Incubations of M-CHO. M-CHO (10 μM) was selected as the substrate to initiate the reactions, which were conducted similar to the procedure for the in vitro incubations of imrecoxib or M1. The incubations included PBS (without or with NAD, NADP, and NADPH), NADPH-fortified HLMs, and HLCs (with or without NADPH). In addition, to assess the involvement of aldehyde oxidase (AOX) on the oxidation of M-CHO, specific-chemical inhibitor menadione (20 and 100 μM) was added to HLC incubations. Reaction phenotyping studies of M-CHO were conducted as described for imrecoxib.

M-CHO Reduction or Oxidation in HLMs. M-CHO (10 μM) was incubated separately with recombinant POR, human CYP3A4R, and human CYP3A4BLR in the presence of NADPH; these conditions were similar to the protocol for HLM incubations of M-CHO. The effect of α-lipoic acid, a selective inhibitor of POR, was assessed at 0, 5, 10, 25, and 50 mM.

Kinetic Analysis. In this study, kinetic analyses involved 1) the conversion of the parent drug to M1 in HLMs; 2) its subsequent oxidation to M-CHO in HLMs or HLCs; 3) conversion of M-CHO to M2 in HLMs (c1), HLCs (c2), or NADPH-fortified HLCs (c3); and 4) competing reduction of M-CHO back to the primary M1 in HLMs or NADPH-fortified HLCs. For V_{max} and K_m determinations, all substrates (imrecoxib, M1, and M-CHO) were incubated at the initial rate in selected concentration ranges, after optimization of incubation time and protein concentrations for the linearity of metabolite formation and <20% of parent depletion (Table 1).

Nonlinear regression analysis of kinetic data was performed using GraphPad Prism software (version 6.01; GraphPad Software Inc., La Jolla, CA). The models fitted included allosteric sigmoidal, substrate inhibition, and Michaelis–Menten models. The goodness-of-fit criteria included a high level of squared correlation coefficients (R^2) as well as appropriate visual inspection of the data. Intrinsic clearance values were calculated as V_{max}/K_m, where V_{max} is the maximum velocity and K_m is the Michaelis constant.

Results

Characterization of Imrecoxib Metabolites in Human Plasma and Urine. A total of 22 metabolites in humans were detected after a single oral administration of 100 mg imrecoxib (Supplemental Table 1). Metabolic profiles of imrecoxib in human plasma and urine are shown in Fig. 1. M1 and M2 were confirmed using reference standards. In plasma, M1 and M2 were the major circulating substances in addition to the parent drug. The systemic exposure ratio of imrecoxib, M1, and M2 was approximately 1:1:4 (Supplemental Table 2). Other minor pathways, such as the hydroxylation of pyrrole and the ω-1 position of the *N*-alkyl chain, were also identified.

Investigation of the Metabolism of Imrecoxib and M1 In Vitro. HLMs, HLCs, and human hepatocytes were selected as the incubation models for exploring the metabolism of imrecoxib in vitro. M0 was mostly oxidized to M1 in HLMs supplemented with NADPH and was accompanied by minor amounts of M2, which accounted for less than 2% of the total metabolites. The addition of ABT in HLMs significantly decreased the formation of the two metabolites by almost 97%, indicating the contribution of P450s to the conversion. The same phenomenon could be observed in the incubation of M0 with human hepatocytes, in which more than 30% of the parent drug was oxidized to M1. By contrast, no metabolites could be detected in HLC incubation with M0, showing that HLC enzymes are not involved in this biotransformation (Fig. 2A).

The formation of M2 originated from the direct conversion of M1 but not of M0, as demonstrated by the limited amount of M2 detected in NADPH-supplemented HLMs or human hepatocytes with M0. To investigate this possibility, M1 was incubated in the same in vitro systems as M0. Compared with those observed in M0 incubations, M2 yields increased, and M2 could be detected in HLC incubation (Fig. 2B). These observations confirmed that M2 was generated from M1 instead of M0. However, regardless of the incubation conditions, the M2 yield remained extremely low.

Elucidation of the Formation of M-CHO. In general, the metabolic intermediates or metabolites with an aldehyde group are generated when the hydroxyl fraction of the compound is oxidized to its corresponding carboxylic acid forms (Diao et al., 2013; Liu et al., 2015; Zhu et al., 2016). Thus, trapping experiments were performed to probe the presence of the aldehyde intermediate. Methoxyamine was used as the trapping agent. A chromatographic peak with the expected $[M+H]^+$ ion at *m/z* 413.150 (Fig. 3A) and the corresponding supportive fragment ions of *m/z* 381.128, 355.125, and 278.084 (Fig. 3C) were observed when M1 and NADPH-fortified HLMs were coincubated with methoxyamine. A significant decrease in M2 yield relative to that of the incubations in the absence of the trapping agent was also observed. The M-CHO–methoxyamine adduct was also detected when the same investigation was conducted with HLCs (Fig. 3B). The results confirmed that M1 is oxidized to M-CHO prior to M2 formation in both HLM and HLC incubations.

To explore the formation of M-CHO, M1 was incubated under different conditions, and the formed M-CHO (*m/z* 384.2→236.2) and M2 (*m/z* 400.2→236.2) were directly detected using a liquid chromatography–MS/MS system in multiple reaction monitoring scan mode. M-CHO was not able to be detected when M1 was incubated in PBS (Fig. 4A), regardless of the addition of coenzyme NAD, NADP, and NADPH. Meanwhile, no M2 was formed (data not shown). In the NADPH-fortified HLM incubations with M1, M-CHO was observed to accompany the M2 yield (Fig. 4B); upon the addition of ABT, the levels of the two metabolites in HLMs markedly decreased (Fig. 4C). In the M1 HLC incubations without NADPH, M2 was detected rather than M-CHO (Fig. 4D), indicating that M-CHO was immediately oxidized to M2 upon formation. These results showed that P450 and HLC enzymes were both responsible for the M-CHO formation.

Metabolic Characteristics of M-CHO. To obtain further insight into M-CHO metabolism, this metabolic intermediate was synthesized to initiate the incubation experiments. An unexpectedly large amount of M2 was generated when M-CHO was incubated with HLCs, whereas M2 together with M1 was considerably formed in NADPH-fortified

TABLE 1

Kinetic analyses for imrecoxib oxidation, M1 oxidation, M-CHO oxidation, and reduction in HLMs, HLCs, or NADPH-fortified HLCs

Substrate	Metabolite	Incubation	Protein Concentration	Incubation Time	Concentration Range	V_{max}	K_m	Intrinsic Clearance
			mg/ml	*min*	*μM*	*pmol/min per mg protein*	*μM*	*μl/min per mg protein*
Imrecoxib	M1	HLM (NADPH)	0.02	60	0.01–100	296	3.72	79.6
M1	M-CHO	HLM (NADPH)	0.10	60	0.25–2500	137	979	0.140
M1	M-CHO	HLC	0.10	60	0.25–2500	33.9	1299	0.0261
M-CHO	M1	HLM (NADPH)	0.04	45	0.01–100	725	8.01	90.5
M-CHO	M2	HLM (NADPH)	0.04	45	0.01–100	2780	56.9	48.9
M-CHO	M2	HLC	0.04	45	0.01–30	209	1.30	161
M-CHO	M1	HLC (NADPH)	0.02	10	0.01–100	973	1.34	727
M-CHO	M2	HLC (NADPH)	0.02	10	0.01–100	39,195	430	91.2

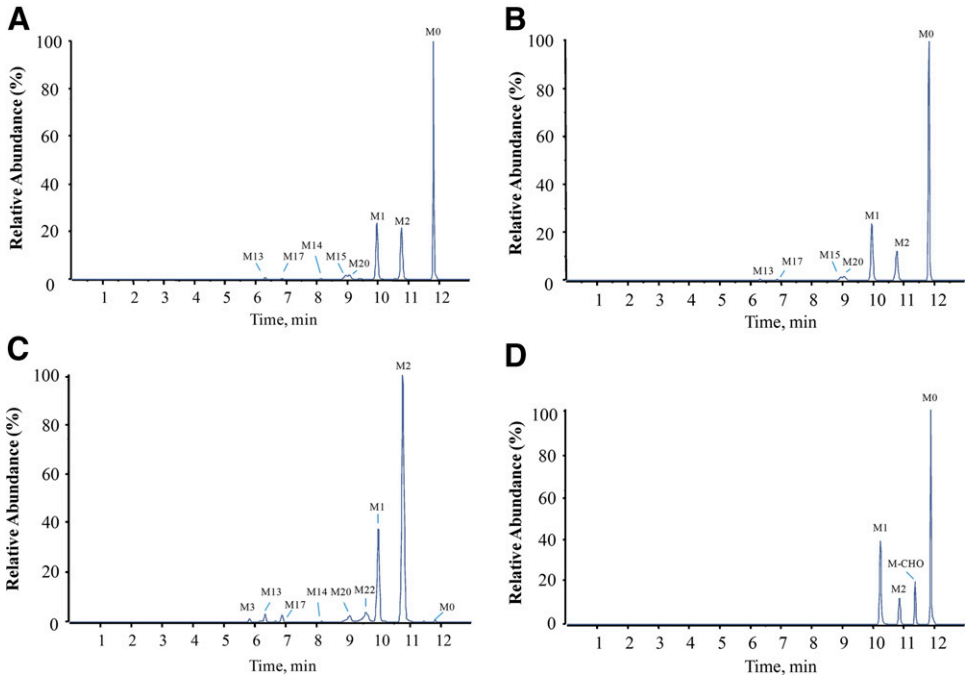

Fig. 1. Metabolic profiles (presented in extracted ion chromatograms) after oral administration of 100 mg imrecoxib. (A–C) Relative abundance in a pooled plasma sample at 1 hour postdose (A) and at 4 hours postdose (B) and in a pooled urine sample at 0–24 hours postdose (C). (D) Chromatogram of the reference substances of imrecoxib, M1, M2, and M-CHO.

HLM incubations (Fig. 5). Moreover, M-CHO was almost depleted in these in vitro incubations. By striking contrast, less M1 was metabolized when it was selected as the substrate. Thus, we concluded that in enzymatic catalysis, the generation of M-CHO from M1 is the rate-limiting step for M2 formation. The in vitro kinetic study provided more direct evidence (Table 1). Intrinsic clearance values for M1 oxidation to M-CHO were minimal whether in HLM or HLC incubations, and the K_m values of this rate-limiting step were markedly higher than those of other metabolic processes.

NADPH-Dependent Effects in Different Subcellular Fractions for M2 Formation. Interestingly, M1 and M-CHO metabolism were influenced significantly by coenzymes, especially NADPH (Figs. 4E and 5). In HLC incubations, M-CHO was almost completely biotransformed into M2. However, upon the addition of NADPH in HLC

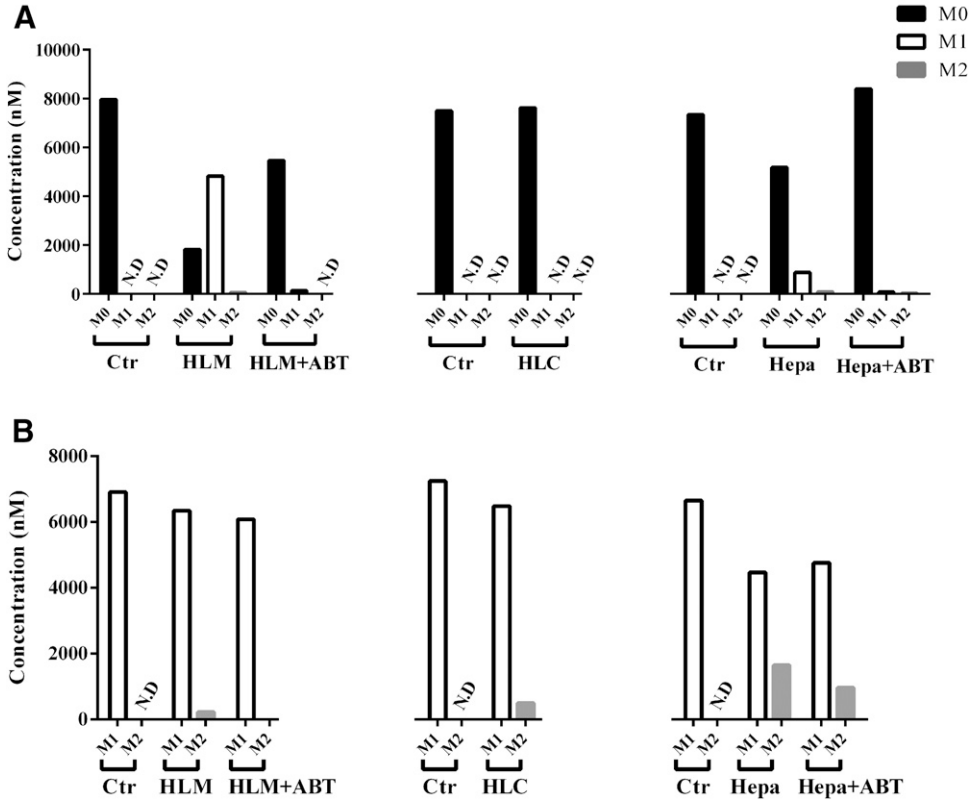

Fig. 2. Comparison of the amounts of M1 and M2 formed in different in vitro incubations, including NADPH-fortified HLMs with or without the addition of P450 inhibitor ABT (left), HLCs (middle), and human hepatocytes with or without ABT (right). (A) M0 (10 μM) as the substrate. (B) M1 (10 μM) as the substrate. Each column represents the mean of duplicate incubations. Ctr, control; Hepa, human hepatocyte; N.D., not detectable.

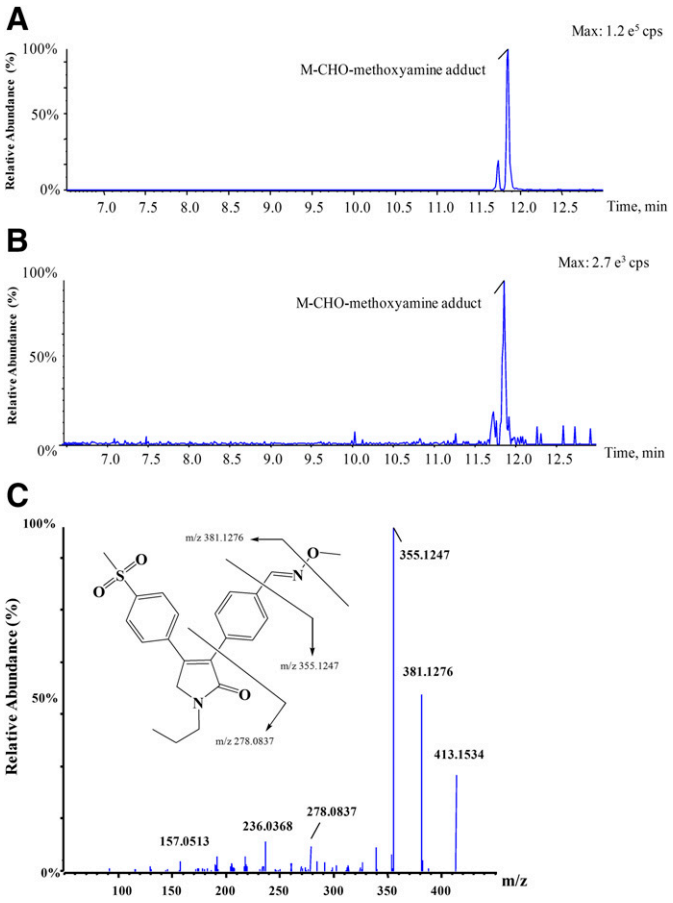

Fig. 3. (A–C) Extract ion chromatograms of the M-CHO–methoxyamine adduct in NADPH- and methoxyamine-supplemented HLMs with M1 (A) and methoxyamine-supplemented HLCs with M1 (B), and a product ion scan spectrum of M-CHO adduct (C). The inset is the tentative fragmentation pattern.

incubations, M2 formation was markedly reduced and accompanied by M1 production (Fig. 5A).

When M-CHO was added to NADPH-fortified HLM incubations, M1 was also detected in addition to M2 at a ratio of 1:2 (Fig. 5B). However, in NADPH-supplemented PBS incubations with M-CHO, neither M1 nor M2 was detected. These data indicated that M-CHO underwent opposite metabolic reactions (i.e., oxidation versus reduction). In addition, the formation of reductive metabolite M1 in these subcellular fractions was dependent on the presence of the cofactor NADPH.

The formation mechanism of M1 in the incubations of M-CHO with NADPH-supplemented HLMs was further investigated. In recombinant NADPH-POR incubations, M-CHO was completely metabolized to M1 instead of M2, suggesting that POR was responsible for the reduction of M-CHO to M1. α-Lipoic acid was effective in inhibiting M1 formation when a 10-fold molar excess of the inhibitor over M-CHO was used (Fig. 6), further supporting the role of POR in the reduction of M-CHO in HLMs.

In addition, in common NADPH-fortified recombinant human CYP3A4 (containing POR and cytochrome-b_5) incubation with M-CHO, both M2 and M1 could be detected at a ratio of 36:1; in human CYP3A4R (without cytochrome-b_5) and human CYP3A4BLR (containing cytochrome-b_5 but low POR activity) incubations in the presence of NADPH, a significant decrease in M2 was observed and a large amount of M1 was obtained instead with the generation ratios of M2 and M1 of 0.4:1 and 0.1:1, respectively (Fig. 7). The results suggested that the oxidation to M2 and reduction to M1 from M-CHO were two competitive pathways. POR and cytochrome-b_5 are both indispensable electron transporters for the oxidation effect of P450 enzymes. The integrity of the electron transport chain (ETC) of P450s might accelerate the M-CHO oxidation pathway, whereas ETC deficiency (e.g., the low activity of POR or the absence of cytochrome-b_5) leads to attenuated oxidation and drives the reduction reaction.

The reducing enzyme(s) involved in the formation of M1 from M-CHO in HLCs is yet to be characterized, because specific inhibitors of several HLC-reducing enzymes, including alcohol dehydrogenase, aldo-keto reductase, quinone reductase, and glutathione peroxidase, cannot inhibit the formation of M1 when M-CHO is incubated in NADPH-supplemented HLCs (data not shown).

Identification of Oxidative Enzymes Responsible for the Formation of M1, M-CHO, and M2. The formation of M1 is P450 mediated. To identify the P450 isoforms, 10 isoforms of recombinant human P450 isozymes were individually incubated with M0. Given that M1 is both the metabolite of M0 and the substrate of M2 in HLMs, the same metabolic enzymes might be shared by the two metabolic steps, causing underestimation of M1 yield. Therefore, the reduction of M0 was monitored to calculate the contribution of individual human P450 enzymes under the condition that the other minor metabolic pathways of M0 were ignored. CYP3A4, CYP2D6, and CYP3A5 were identified as the principal catalyzing enzymes (Fig. 8A). After normalization for the relative hepatic abundance of P450 enzymes, the relative contributions of CYP3A4 and CYP2D6 were calculated as 68% and 32%, respectively. Specific-chemical inhibition tests also provided further supporting data (Supplemental Fig. 1).

The same method was applied to evaluate P450 enzyme(s) catalysis of M-CHO to M2. CYP3A4 was confirmed to be the most active enzyme for M2 formation, followed by CYP2D6, with contributions of 61% and 38%, respectively (Fig. 8B). M2 can be detected when M-CHO is incubated with HLC. Aldehyde dehydrogenase (ALDH), AOX, and xanthine oxidase (XO) are the main oxidases for aldehyde compounds in liver cytosol. XO always catalyzes the metabolism of endogenous substances or purine analogs, whereas the structures of imrecoxib and its metabolites do not meet the requirement. In addition, ALDH was noneffective for oxidation in the absence of NADP, whereas M-CHO could be depleted in HLCs without any cofactors. Thus, XO and ALDH were disregarded in this experiment. A specific inhibitor was added in HLCs to only identify the possible AOX being responsible for M2 formation. The yield of M2 in HLCs was attenuated by up to 25% and 95% by 20 and 100 μM menadione (an AOX inhibitor), respectively. The data indicated that AOX was the most efficient enzyme involved in the formation of M2 in HLCs.

To determine which P450 enzyme(s) preferentially oxidize M1 to M-CHO, we performed trapping experiments and investigated the formation of M-CHO adduct in different recombinant human P450 enzymes. The results indicated that CYP3A4, CYP2D6, and CYP3A5 were the key P450 enzymes responsible for the formation of M-CHO, with a ratio of 2:6:1. However, the contributions of the three P450s might be overestimated, because these isoforms can also catalyze further oxidation of M-CHO. In the HLC incubations with M1, M-CHO could not be detected because the formation rate of M2 was considerably higher than that of M-CHO. As a result, the cytosolic enzyme(s) responsible for the oxidation of M1 to M-CHO could not be identified.

Investigation of M2 Formation in Rats. To characterize M2 formation in vivo, imrecoxib, M1, and M-CHO were directly administered

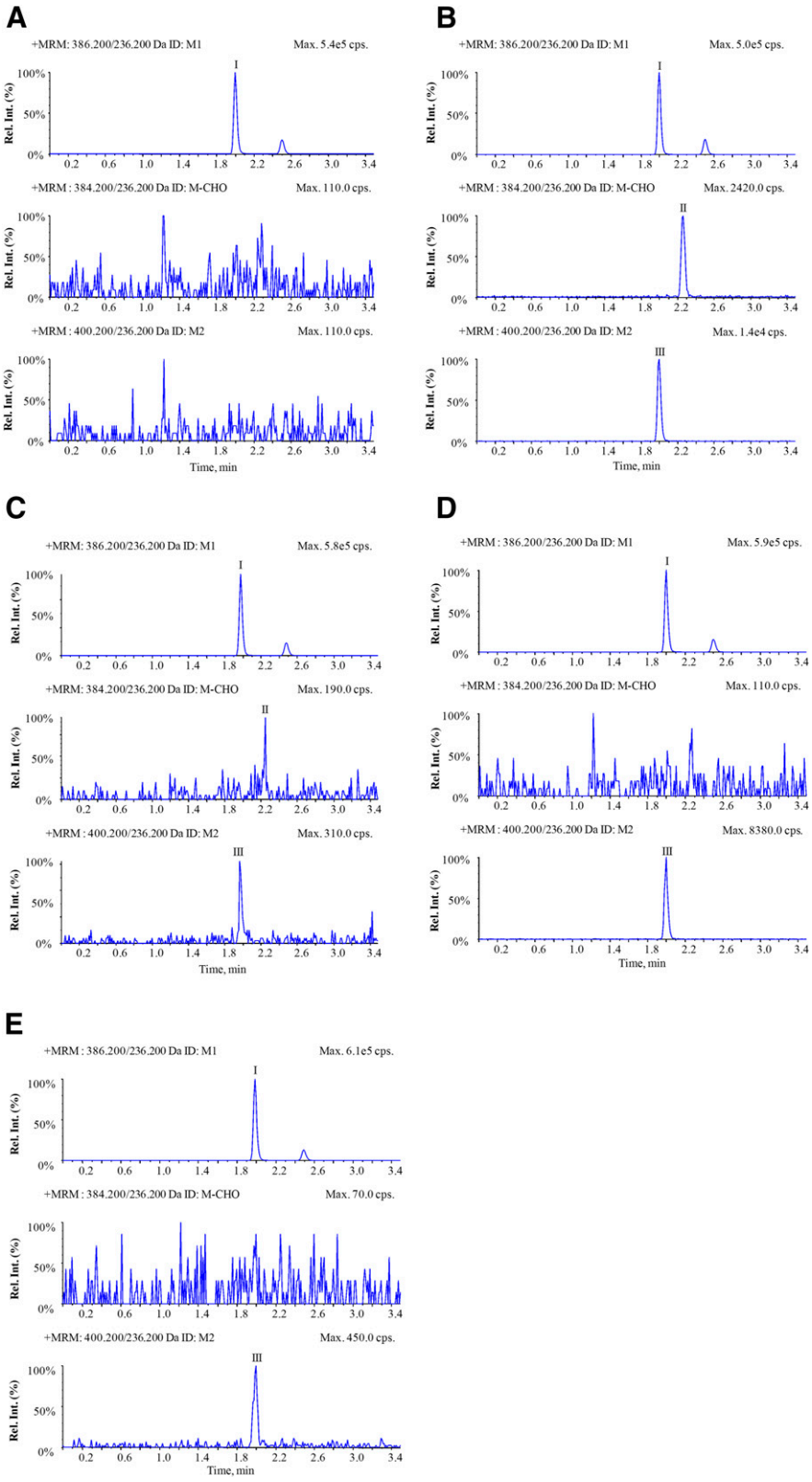

Fig. 4. (A–E) Chromatograms of liquid chromatography–MS analyses of M1 (1.5 μM) metabolism in PBS (A), NADPH-fortified HLMs (B), NADPH- and ABT-supplemented HLMs (C), HLCs (D), and NADPH-fortified HLCs (E). Peaks I–III represent M1, M-CHO, and M2, respectively. MRM, multiple reaction monitoring; Rel. Int., relative intensity.

by intravenous injection to Sprague-Dawley rats, respectively. The mean plasma concentration-time curves of M2 are presented in Supplemental Fig. 2. After intravenous administration of M-CHO, M1, and imrecoxib, peak plasma concentrations were reached at 0.083, 0.5, and 1 hours postdose with mean values of 1013, 902, and 437 ng/ml. The area under the plasma concentration-time curve from zero to 10 hour values were comparable, with 1073, 1193, and 736 ng·h/ml, respectively.

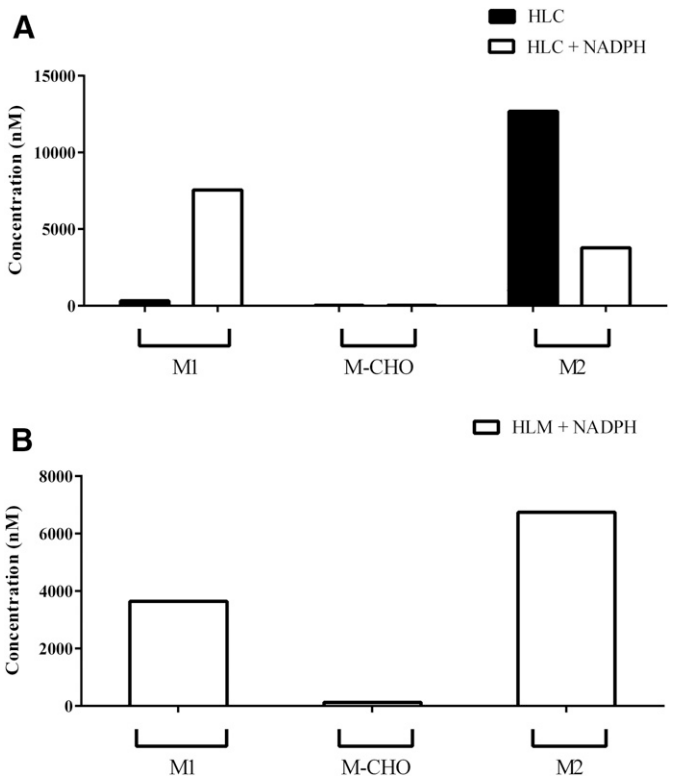

Fig. 5. (A and B) Effect of the cofactor NADPH on the metabolism of M-CHO (10 μM) in HLC (A) and HLM (B) incubations. Each column represents the mean of duplicate incubations.

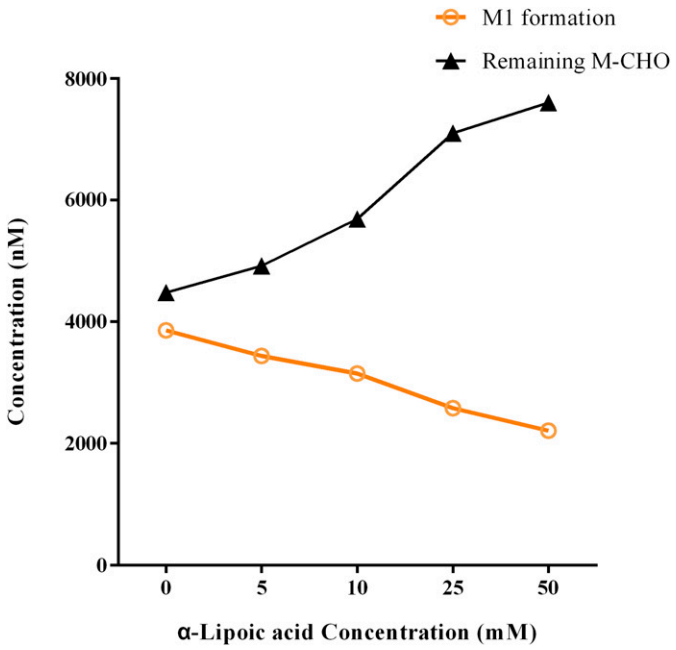

Fig. 6. Effect of α-lipoic acid concentrations on the formation of M1 in the recombinant human POR incubation containing M-CHO (10 μM), NADPH, and α-lipoic acid.

Discussion

The carboxylic acid metabolite M2 appears to be the major metabolite of imrecoxib in plasma and urine, accounting for 68% of the systemic exposure and 77% for the total clearance, respectively. However, M2 is not generated to any significant extent in typical in vitro metabolic models, including HLMs, HLCs, and human hepatocytes. The key metabolic process being responsible for M2 formation is expected to be investigated.

The origin of M2 should be defined first because the end-stage metabolite may be directly generated from the parent drug (Xie et al., 2013; Mu et al., 2014) or may undergo successive multistep metabolic pathways (Zhou et al., 2015). In this study, the major metabolic pathway of imrecoxib was characterized as M0 being successively oxidized to M1, to M-CHO, and ultimately to M2, because more M2 was observed in the M1 incubations relative to M0 incubations, and trapping experiments with methoxyamine provided further evidence. The kinetic analyses indicated that the biotransformation from M1 to M-CHO was the rate-limiting step for M2 generation. On the contrary, in in vivo conditions, the formation of M2 was comparable after intravenous administration of imrecoxib, M1, and M-CHO, suggesting that the barrier of M-CHO formation was easy to overcome under dynamic and physiologic situations. Thus, the discrepancy between in vivo and in vitro for M-CHO formation may be the key point for explaining why only minor amounts of M2 were formed during in vitro incubation of imrecoxib.

NADPH is often used as a cofactor in in vitro metabolism investigations for donating electrons. NADPH participates in the oxidation or the reduction based on the electron transport. In NADPH-fortified HLM incubations with M-CHO, the oxidative metabolite M2, as well as the reductive metabolite M1, could be detected. The phenomenon also emerged in recombinant CYP3A4 incubations. In general, most marketed recombinant human P450 enzymes contain NADPH-POR and cytochrome-b_5 to enhance the activity of enzymes because the two components are the major electron transporters of ETC (Aigrain et al., 2011; Kenaan et al., 2011). Meanwhile, POR can directly mediate the one-electron reductive biotransformation, such as the nitro reduction of aristolochic acid (Henderson et al., 2003; Stiborová et al., 2005, 2011). In this study, POR could catalyze the reduction of M-CHO back to M1. Compared with CYP3A4 incubation, M2 production significantly decreased with the increase in M1 in human CYP3A4R and CYP3A4BLR incubations with M-CHO. Therefore, it was inferred that the NADPH-dependent POR expressed dual effects, including both oxidation and reduction on M-CHO in HLMs by donating electrons to microsomal P450s or directly to the substrate M-CHO. M1 incubation in NADPH-fortified HLMs generated M-CHO, which can be further oxidized to M2 and reduced back to M1 simultaneously in two competitive pathways.

M-CHO was rapidly metabolized with AOX mediation to M2 in HLCs, whereas a significant decrease existed in M2 formation in NADPH-fortified HLCs. Holm et al. (2016) reported that JWH-018 [1-pentyl-3-(1-naphthoyl)indole], a marketed synthetic cannabinoid, can be oxidized to JWH-018 ω–COOH in HLCs, whereas the process can be nearly terminated completely by adding NADPH. However, the authors did not explain the cause of prevention by this cofactor. As seen in this study, M-CHO can be reduced back to M1 in HLCs in the presence of NADPH, causing the attenuation of the oxidation to M2. However, the NADPH-dependent enzyme(s) in HLCs responsible for the M-CHO reduction remains to be identified.

Drugs containing the benzylic carbon motif are prone to be oxidized to its corresponding benzylic alcohol (Mamidi et al., 2014; Ryu et al., 2014) and/or further to the end-product carboxylic acids in vivo (Hvenegaard et al., 2012; Walles et al., 2013; Pozo et al., 2015). It is recognized that there is an aldehyde intermediate in metabolic processing from alcohol to carboxylic acid, and some in vitro trapping tests with methoxyamine or semicarbazide also

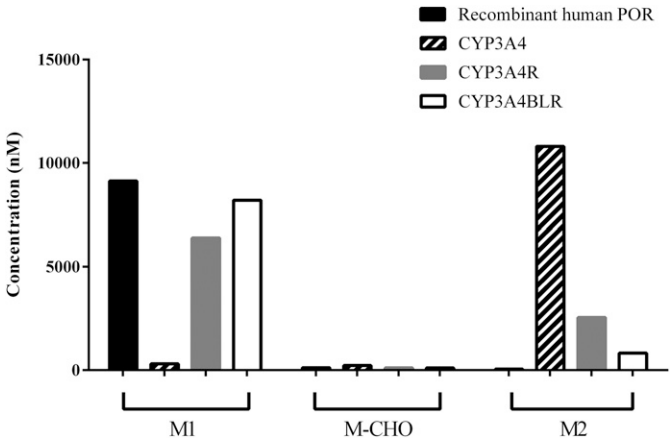

Fig. 7. Formation of M1 and M2 in M-CHO incubations with recombinant human POR, CYP3A4 (containing POR and cytochrome-b_5), CYP3A4R (without cytochrome-b_5), and CYP3A4BLR (containing cytochrome-b_5, but with low POR activity). All incubations were supplemented with NADPH. Data are displayed as the means of two separate samples.

provided convincing evidence (Li et al., 2014; Inoue et al., 2015; Liu et al., 2015). However, further metabolism of aldehyde intermediates is rarely reported in publications. Dopamine is a special case that undergoes oxidative deamination initially to aldehyde (3,4-dihydroxyphenylacetaldehyde), followed by ALDH-mediated oxidation to phenylacetic acid metabolite and reductase-mediated reduction to phenylethanol metabolite (Jinsmaa et al., 2009). Different from M-CHO, 3,4-dihydroxyphenylacetaldehyde was reduced to a new forward metabolite, not its precursor dopamine.

In vitro metabolism incubations (e.g., subcellular fractions) occur in a static system, representing only a few of several dimensions of a complex in vivo system (Wang et al., 2010; Subramanian et al., 2013). Several drugs, such as linezolid and ziprasidone, are metabolized through multiple sequential reactions in vivo, whereas they can only undergo one or two sequential reactions in in vitro systems (Wang et al., 2010), especially when a metabolic intermediate is generated. Furthermore, even if the intermediate M-CHO can be partially reduced to M1 in vivo, this reduced product might enter into other subcellular fractions, such as kidney microsomes or cytosol, where M1 might be easily oxidized again in the absence of NADPH-dependent cytosolic reductase(s) similar to the liver (Brandon et al., 2003; Marchitti et al., 2008; Argikar et al., 2016). This was further supported by the in vitro data. M2 could be generated in M1 incubations with human renal homogenate, as well as rat renal homogenate (Supplemental Fig. 3). In rats, peak time of M2 plasma concentrations was gradually postponed after intravenous administration of M-CHO, M1, and imrecoxib, and no significant difference in plasma exposure of M2 was observed among three groups. These results indicated that the metabolite M1 derived from imrecoxib could circulate continuously into the liver or other metabolic organs and could be removed from the body in the form of the end-product M2. By contrast, in static in vitro incubations, M1 failed to accomplish a similar process to the dynamic in vivo system, and the formed M1 was not reused.

It was observed that M1 and M-CHO could interconvert into each other via oxidation or reduction in HLCs as well as in HLMs. However, the two metabolic processes are not real reversible reaction steps, because these conversions occurred under different conditions. In HLMs, the conversion of M1 to M-CHO was catalyzed by P450s, whereas the reduction of M-CHO to M1 was catalyzed by POR. In HLCs, these two metabolic pathways were mediated by NADPH-independent enzymes and NADPH-dependent enzymes, respectively.

Li et al. (2005) reported that CYP2C9 was the major enzyme involved in imrecoxib hydroxylation metabolism, along with CYP2D6 and CYP3A4. In our study, recombinant human CYP2C9 incubation assays and the HLM inhibition experiment with specific-chemical inhibitor sulfaphenazole both confirmed that CYP2C9 was not responsible for the oxidation of imrecoxib as well as M1 and M-CHO.

In conclusion, this study demonstrates that the extensive oxidative metabolism of imrecoxib occurred primarily on its benzylic carbon motif to generate M1 and M2 by a two-step successive oxidization (Fig. 9). The initial hydroxylation was mainly mediated by CYP3A4 and CYP2D6, with relative contributions of 68% and 32%, respectively, to form M1 in HLMs. M1 was then oxidized to M-CHO in HLMs and HLCs. Meanwhile, this process was the rate-limiting step in the generation of the end-product M2. Two opposite reactions occurred in further M-CHO metabolism—namely, rapid oxidation to form M2, which was catalyzed by CYP3A4, CYP2D6, and cytosol enzyme AOX, versus reduction to regenerate M1, which was catalyzed by an NADPH-dependent reductase in HLMs and HLCs, such as P450 reductase. Thus, the amount of M2 in static in vitro incubations was

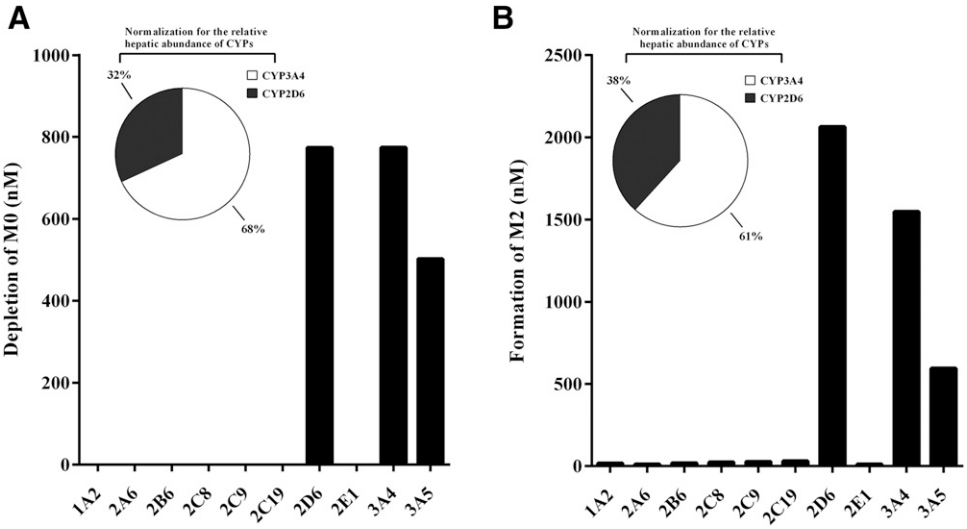

Fig. 8. (A and B) Incubation of imrecoxib (A) and M-CHO (B) in recombinant human P450 enzymes in the presence of NADPH. Each bar represents the mean of two separate samples.

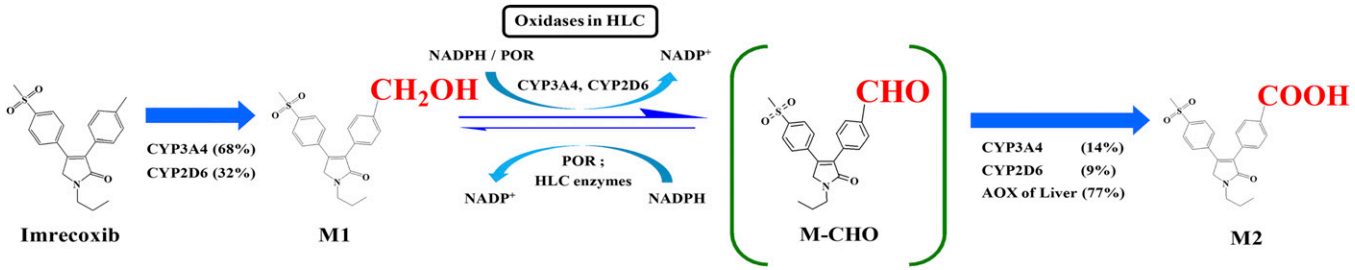

Fig. 9. Proposed formation mechanism of M1 and M2, the major metabolites of imrecoxib in humans.

considerably underestimated. These findings presented one of the explanations for the discrepancy between in vitro and in vivo metabolic data, and the investigation prompted that the effect of competitive reduction on the static oxidation metabolism should be considered in in vitro metabolic experiments.

Acknowledgments

We thank Fubao Huang for help with synthesis of the M-CHO reference substance. We also thank the clinical staff of the Xijing Hospital affiliated with the Fourth Military Medical University and the volunteers in this clinical study.

Authorship Contributions

Participated in research design: Hou, J. Zhou, L. Zhou, Zhang, Zhong, Chen.

Conducted experiments: Hou, J. Zhou, Yu.

Contributed new reagents or analytic tools: Hou, J. Zhou, Yu, Zhang, Zhong, Chen.

Performed data analysis: Hou, L. Zhou, Chen.

Wrote or contributed to the writing of the manuscript: Hou, L. Zhou, Chen.

References

Aigrain L, Pompon D, and Truan G (2011) Role of the interface between the FMN and FAD domains in the control of redox potential and electronic transfer of NADPH-cytochrome P450 reductase. *Biochem J* **435**:197–206.

Argikar UA, Potter PM, Hutzler JM, and Marathe PH (2016) Challenges and Opportunities with Non-CYP Enzymes Aldehyde Oxidase, Carboxylesterase, and UDP-Glucuronosyltransferase: Focus on Reaction Phenotyping and Prediction of Human Clearance. *AAPS J* **18**:1391–1405.

Brandon EF, Raap CD, Meijerman I, Beijnen JH, and Schellens JH (2003) An update on in vitro test methods in human hepatic drug biotransformation research: pros and cons. *Toxicol Appl Pharmacol* **189**:233–246.

Diao X, Deng P, Xie C, Li X, Zhong D, Zhang Y, and Chen X (2013) Metabolism and pharmacokinetics of 3-n-butylphthalide (NBP) in humans: the role of cytochrome P450s and alcohol dehydrogenase in biotransformation. *Drug Metab Dispos* **41**:430–444.

Feng Z, Chu F, Guo Z, and Sun P (2009) Synthesis and anti-inflammatory activity of the major metabolites of imrecoxib. *Bioorg Med Chem Lett* **19**:2270–2272.

Henderson CJ, Otto DME, Carrie D, Magnuson MA, McLaren AW, Rosewell I, and Wolf CR (2003) Inactivation of the hepatic cytochrome P450 system by conditional deletion of hepatic cytochrome P450 reductase. *J Biol Chem* **278**:13480–13486.

Holm NB, Noble C, and Linnet K (2016) JWH-018 ω-OH, a shared hydroxy metabolite of the two synthetic cannabinoids JWH-018 and AM-2201, undergoes oxidation by alcohol dehydrogenase and aldehyde dehydrogenase enzymes in vitro forming the carboxylic acid metabolite. *Toxicol Lett* **259**:35–43.

Hvenegaard MG, Bang-Andersen B, Pedersen H, Jørgensen M, Püschl A, and Dalgaard L (2012) Identification of the cytochrome P450 and other enzymes involved in the in vitro oxidative metabolism of a novel antidepressant, Lu AA21004. *Drug Metab Dispos* **40**: 1357–1365.

Inoue K, Fukuda K, Yoshimura T, and Kusano K (2015) Comparison of the reactivity of trapping reagents toward electrophiles: cysteine derivatives can be bifunctional trapping reagents. *Chem Res Toxicol* **28**:1546–1555.

Jinsmaa Y, Florang VR, Rees JN, Anderson DG, Strack S, and Doorn JA (2009) Products of oxidative stress inhibit aldehyde oxidation and reduction pathways in dopamine catabolism yielding elevated levels of a reactive intermediate. *Chem Res Toxicol* **22**: 835–841.

Kenaan C, Zhang H, Shea EV, and Hollenberg PF (2011) Uncovering the role of hydrophobic residues in cytochrome P450-cytochrome P450 reductase interactions. *Biochemistry* **50**:3957–3967.

Li F, Lu J, and Ma X (2014) CPY3A4-mediated α-hydroxyaldehyde formation in saquinavir metabolism. *Drug Metab Dispos* **42**:213–220.

Li Q, Huang HH, Dong Y, and Zhong DF (2005) [Investigation on the hydroxylation metabolism of imrecoxib in vitro by using recombinant human CYPs]. *Yao Xue Xue Bao* **40**:912–915.

Liu X, Lu Y, Guan X, Dong B, Chavan H, Wang J, Zhang Y, Krishnamurthy P, and Li F (2015) Metabolomics reveals the formation of aldehydes and iminium in gefitinib metabolism. *Biochem Pharmacol* **97**:111–121.

Mamidi RN, Cuyckens F, Chen J, Scheers E, Kalamaridis D, Lin R, Silva J, Sha S, Evans DC, Kelley MF, et al. (2014) Metabolism and excretion of canagliflozin in mice, rats, dogs, and humans. *Drug Metab Dispos* **42**:903–916.

Marchitti SA, Brocker C, Stagos D, and Vasiliou V (2008) Non-P450 aldehyde oxidizing enzymes: the aldehyde dehydrogenase superfamily. *Expert Opin Drug Metab Toxicol* **4**:697–720.

Mu P, Zheng M, Xu M, Zheng Y, Tang X, Wang Y, Wu K, Chen Q, Wang L, and Deng Y (2014) N-oxide reduction of quinoxaline-1,4-dioxides catalyzed by porcine aldehyde oxidase SsAOX1. *Drug Metab Dispos* **42**:511–519.

Paulson SK, Hribar JD, Liu NW, Hajdu E, Bible RH, Jr, Piergies A, and Karim A (2000) Metabolism and excretion of [(14)C]celecoxib in healthy male volunteers. *Drug Metab Dispos* **28**:308–314.

Pozo OJ, Ibáñez M, Sancho JV, Lahoz-Beneytez J, Farré M, Papaseit E, de la Torre R, and Hernández F (2015) Mass spectrometric evaluation of mephedrone in vivo human metabolism: identification of phase I and phase II metabolites, including a novel succinyl conjugate. *Drug Metab Dispos* **43**:248–257.

Rodrigues AD (1999) Integrated cytochrome P450 reaction phenotyping: attempting to bridge the gap between cDNA-expressed cytochromes P450 and native human liver microsomes. *Biochem Pharmacol* **57**:465–480.

Rodrigues AD, Halpin RA, Geer LA, Cui D, Woolf EJ, Matthews CZ, Gottesdiener KM, Larson PJ, Lasseter KC, and Agrawal NG (2003) Absorption, metabolism, and excretion of etoricoxib, a potent and selective cyclooxygenase-2 inhibitor, in healthy male volunteers. *Drug Metab Dispos* **31**:224–232.

Ryu SH, Park BY, Kim SY, Park SH, Jung HJ, Park M, Park KD, Ahn T, Kang HS, and Yun CH (2014) Regioselective hydroxylation of omeprazole enantiomers by bacterial CYP102A1 mutants. *Drug Metab Dispos* **42**:1493–1497.

Sandberg M, Yasar U, Strömberg P, Höög JO, and Eliasson E (2002) Oxidation of celecoxib by polymorphic cytochrome P450 2C9 and alcohol dehydrogenase. *Br J Clin Pharmacol* **54**:423–429.

Stiborová M, Frei E, Hodek P, Wiessler M, and Schmeiser HH (2005) Human hepatic and renal microsomes, cytochromes P450 1A1/2, NADPH:cytochrome P450 reductase and prostaglandin H synthase mediate the formation of aristolochic acid-DNA adducts found in patients with urothelial cancer. *Int J Cancer* **113**:189–197.

Stiborová M, Mares J, Levova K, Pavlickova J, Barta F, Hodek P, Frei E, and Schmeiser HH (2011) Role of cytochromes P450 in metabolism of carcinogenic aristolochic acid I: evidence of their contribution to aristolochic acid I detoxication and activation in rat liver. *Neuroendocrinol Lett* **32** (Suppl 1):121–130.

Subramanian M, Paruchury S, Singh Gautam S, Pratap Singh S, Arla R, Pahwa S, Jana S, Katnapally P, Yoganand V, Lakshmaiah B, et al. (2013) Characterization of recombinantly expressed rat and monkey intestinal alkaline phosphatases: in vitro studies and in vivo correlations. *Drug Metab Dispos* **41**:1425–1432.

Tang C, Shou M, Mei Q, Rushmore TH, and Rodrigues AD (2000) Major role of human liver microsomal cytochrome P450 2C9 (CYP2C9) in the oxidative metabolism of celecoxib, a novel cyclooxygenase-II inhibitor. *J Pharmacol Exp Ther* **293**:453–459.

Tang C, Shou M, Rushmore TH, Mei Q, Sandhu P, Woolf EJ, Rose MJ, Gelmann A, Greenberg HE, De Lepeleire I, et al. (2001) In-vitro metabolism of celecoxib, a cyclooxygenase-2 inhibitor, by allelic variant forms of human liver microsomal cytochrome P450 2C9: correlation with CYP2C9 genotype and in-vivo pharmacokinetics. *Pharmacogenetics* **11**:223–235.

Walles M, Wolf T, Jin Y, Ritzau M, Leuthold LA, Krauser J, Gschwind HP, Carcache D, Kittelmann M, Ocwieja M, et al. (2013) Metabolism and disposition of the metabotropic glutamate receptor 5 antagonist (mGluR5) mavoglurant (AFQ056) in healthy subjects. *Drug Metab Dispos* **41**:1626–1641.

Wang WW, Khetani SR, Krzyzewski S, Duignan DB, and Obach RS (2010) Assessment of a micropatterned hepatocyte coculture system to generate major human excretory and circulating drug metabolites. *Drug Metab Dispos* **38**:1900–1905.

Xie C, Zhou J, Guo Z, Diao X, Gao Z, Zhong D, Jiang H, Zhang L, and Chen X (2013) Metabolism and bioactivation of famitinib, a novel inhibitor of receptor tyrosine kinase, in cancer patients. *Br J Pharmacol* **168**:1687–1706.

Xu H, Zhang Y, Sun Y, Zhang P, Chu F, Guo Z, Zhang H, and Zhong D (2006a) Metabolism and excretion of imrecoxib in rat. *Xenobiotica* **36**:441–455.

Xu HY, Xie ZY, Zhang P, Sun J, Chu FM, Guo ZR, and Zhong DF (2006b) Role of rat liver cytochrome P450 3A and 2D in metabolism of imrecoxib. *Acta Pharmacol Sin* **27**:372–380.

Zhou L, Pang X, Xie C, Zhong D, and Chen X (2015) Chemical and enzymatic transformations of nimesulide to GSH conjugates through reductive and oxidative mechanisms. *Chem Res Toxicol* **28**: 2267–2277.

Zhu Y, Li L, Deng P, Chen X, and Zhong D (2016) Characterization of TPN729 metabolites in humans using ultra-performance liquid chromatography/quadrupole time-of-flight mass spectrometry. *J Pharm Biomed Anal* **117**:217–226.

Address correspondence to: Xiaoyan Chen, Shanghai Institute of Materia Medica, Chinese Academy of Sciences, 501 Haike Road, Shanghai 201203, China. E-mail: xychen@simm.ac.cn

Supplemental data

Manuscript title:

Differences of the *in vivo* and *in vitro* metabolism of imrecoxib in humans: formation of rate-limiting aldehyde intermediate

Authors:

Xiangyu Hou, Jialan Zhou, Songda Yu, Lei Zhou, Yifan Zhang, Dafang Zhong, Xiaoyan Chen

Journal name:

Drug Metabolism and Disposition

Supplemental Figure 1: Effect of specific CYP inhibitors on M0 depletion in HLM incubations containing imrecoxib, NADPH, and individual inhibitor. The control is normalized to 100%.

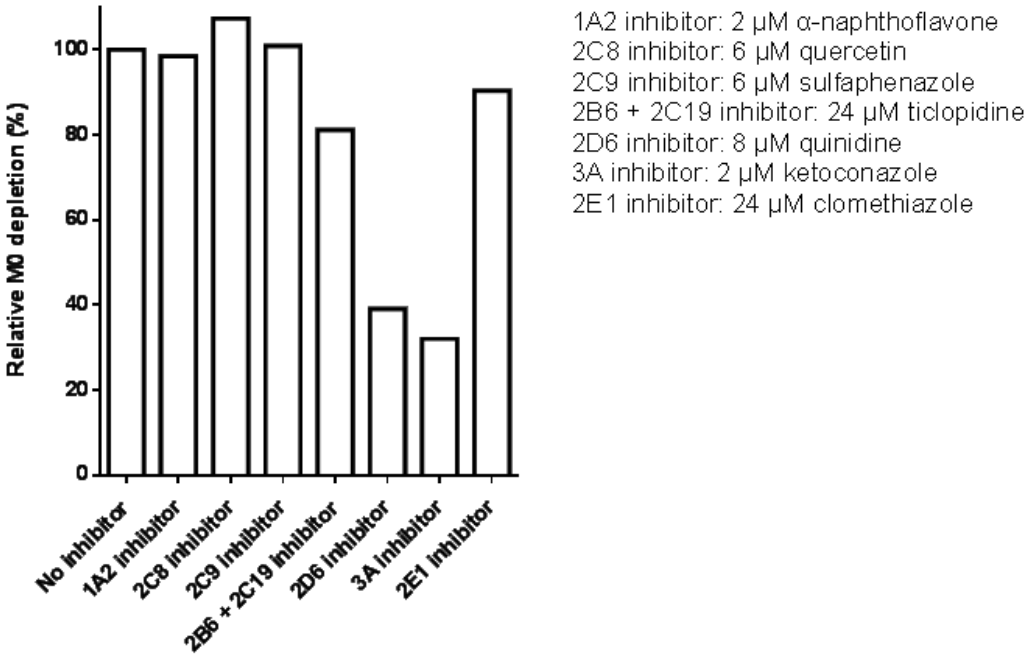

Supplemental Figure 2: Mean plasma concentration-time curves for M2 after a single intravenous administration of 5 mg/kg imrecoxib, M1, and M-CHO, respectively to rats (n = 5/group).

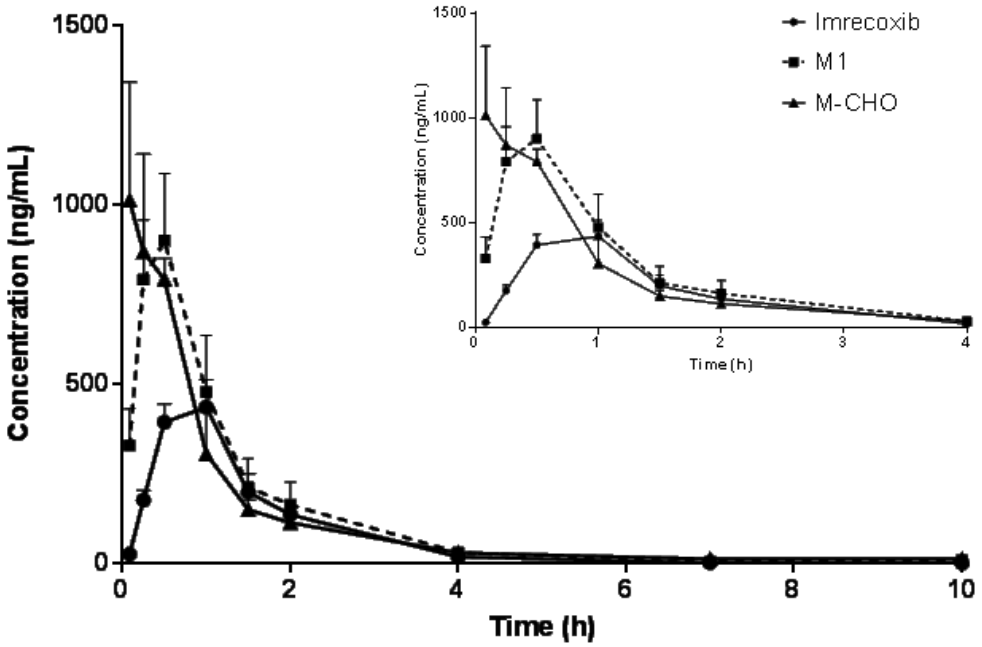

Supplemental Figure 3: Incubations of M1 (10 μM) in NADPH- or NAD-supplemented human renal homogenate (HRH, unknown concentration) (A), and in freshly prepared rat renal and liver homogenate (unknown concentration) for 0.33, 0.5, 1.0, 2.0, 4.0, 6.0 h (B). Each data is displayed as the mean of two separate samples.

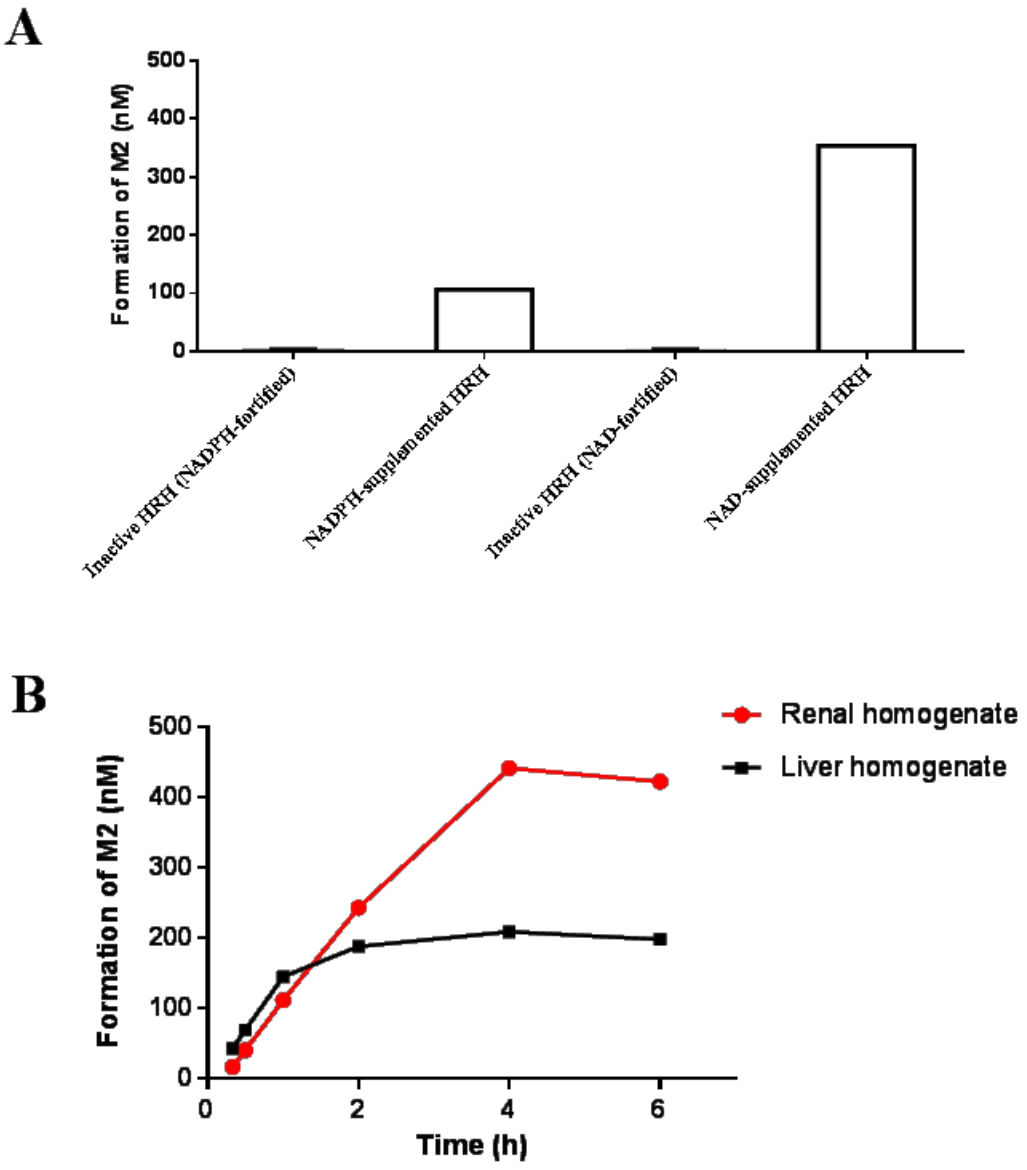

Supplemental Table 1: Characterization of imrecoxib metabolites in humans using UPLC/Q-TOF MS.

Metabolite	Proposed Structure			Retention time (min)	Formula	m/z	ppm	Major product ions
	R1	R2	R3					
M0	CH_3	$CH_2CH_2CH_3$	H	11.8	$C_{21}H_{23}NO_3S$	370.1461	-2.9	278.0821, 236.0353, 157.0501, 129.0552
M1[a]	CH_2OH	$CH_2CH_2CH_3$	H	9.97	$C_{21}H_{23}NO_4S$	386.1414	-1.8	386.1405, 356.1303, 326.0836, 278.0837
M2[a]	COOH	$CH_2CH_2CH_3$	H	10.76	$C_{21}H_{21}NO_5S$	400.1206	-1.9	382.1104, 358.0739, 340.0634, 321.1355
M3	CH_2OH	H	O	5.81	$C_{18}H_{15}NO_5S$	358.0742	-0.6	340.0636, 236.0369, 157.0497
M4	CH_2OH	H	H	5.53	$C_{18}H_{17}NO_4S$	344.0946	-1.3	326.0833, 236.0371
M5	CH_3	$CH_2CH_2CH_3$	OH	10.82	$C_{21}H_{23}NO_4S$	386.1401	-5.0	368.1271, 340.1378, 283.0757, 206.1054
M6[b]	CH_3	$CH_2CH_2CH_3$	O	10.56	$C_{21}H_{23}NO_4S$	386.1420	-0.3	368.1460, 326.0905, 283.0790
M7	CH_3	$CH_2CHOHCH_3$	H	10.4	$C_{21}H_{23}NO_4S$	386.1424	0.9	368.1386, 326.0728, 299.0645
M8[c]	CHO	$CH_2CH_2CH_3$	H	N.A.	$C_{21}H_{21}NO_4S$	N.A.	N.A.	N.A.
M9	CH_2OH	$CH_2CH_2CH_3$	O	6.56	$C_{21}H_{21}NO_5S$	400.1215	0.5	370.1125, 343.0928, 354.1150
M10	CH_2OH	$CH_2CH_2CH_3$	O	11.25	$C_{21}H_{21}NO_5S$	400.1210	-0.9	358.0788, 250.0783, 236.0834
M11[b]	CH_2OH	$CH_2CH_2CH_3$	O	7.81	$C_{21}H_{23}NO_5S$	402.1366	-0.8	384.1250, 356.1354, 309.0523
M12	CH_3	$CH_2CHOHCH_3$	OH	6.15	$C_{21}H_{23}NO_5S$	402.1368	-0.4	384.1245, 356.0933
M13	CH_2OH	$CH_2CH_2CH_3$	OH	6.32	$C_{21}H_{23}NO_5S$	402.1368	-0.3	384.1261, 192.0922
M14	CH_2OH	$CH_2CHOHCH_3$	H	8.14	$C_{21}H_{23}NO_5S$	402.1369	-0.1	384.1259, 343.0647, 271.0776, 183.0107
M15	COOH	$CH_2CHOHCH_3$	H	8.95	$C_{21}H_{21}NO_6S$	416.1152	-2.5	398.1051, 357.0433, 183.0089
M16	CH_2OH	$CH_2CHOHCH_3$	O	8.45	$C_{21}H_{21}NO_6S$	416.1155	-1.8	398.1033, 370.1076, 313.0530, 297.0557
M17				6.86	$C_{21}H_{21}NO_6S$	416.1159	-0.7	398.1055, 370.1106, 297.0581, 236.0828
M18	CH_2OH	CH_2COCH_3	OH	6.64	$C_{21}H_{21}NO_6S$	416.1162	-0.1	398.1049, 370.0716
M19[b]	CH_2OH	CH_2COCH_3	O	6.19	$C_{21}H_{21}NO_6S$	416.1163	0.1	356.0952
M20	$CH_2OC_6H_9O_6$	$CH_2CH_2CH_3$	H	9.05	$C_{27}H_{31}NO_{10}S$	562.1727	-2.5	386.1419, 368.1310
M21	CH_3	$CH_2CHOC_6H_9O_6CH_3$	H	10.92	$C_{27}H_{31}NO_{10}S$	562.1735	-1.2	386.2890, 368.1298
M22	$COOC_6H_9O_6$	$CH_2CH_2CH_3$	H	9.57	$C_{27}H_{29}NO_{11}S$	576.1520	-2.5	400.1206

a. Confirmed using references; b. Nuclear structure is 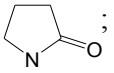 ;

c. Reactive metabolite confirmed by trapping experiment with methoxyamine.

Supplemental Table 2: Pharmacokinetic parameters of imrecoxib and its two active metabolites after an oral administration of 100 mg imrecoxib to healthy volunteers (*n* = 10). Each data presents as mean ± S.D., except for T_{max} [median (range)]. S.D., standard deviation.

Parameter	Unit	Imrecoxib	M1	M2
AUC (0-t)	ng/mL*h	429 ± 387	397 ± 168	1521 ± 634
AUC (0-∞)	ng/mL*h	435 ± 389	411 ± 172	1657 ± 777
C_{max}	ng/mL	48.6 ± 35.4	50.9 ± 16.1	205 ± 83.6
T_{max}	h	1.0 (0.5 - 2.0)	1.0 (0.5 - 3.0)	2.0 (1.0 - 3.0)
$t_{1/2}$	h	10.5 ± 3.71	11.2 ± 7.12	12.5 ± 8.40